University of Nebraska - Lincoln
DigitalCommons@University of Nebraska - Lincoln

Xia Hong Publications | Research Papers in Physics and Astronomy

2006

Ferromagnetism and structure of epitaxial Cr-doped anatase TiO2 thin films

T. C. Kaspar
Pacific Northwest National Laboratory

T. Droubay
Pacific Northwest National Laboratory

V. Shutthanandan
Pacific Northwest National Laboratory

S. M. Heald
Pacific Northwest National Laboratory

C. M. Wang
Pacific Northwest National Laboratory

See next page for additional authors

Follow this and additional works at: https://digitalcommons.unl.edu/physicshong

 Part of the Atomic, Molecular and Optical Physics Commons, and the Engineering Physics Commons

Kaspar, T. C.; Droubay, T.; Shutthanandan, V.; Heald, S. M.; Wang, C. M.; McCready, D. E.; Thevuthasan, S.; Bryan, J. D.; Gamelin, D. R.; Kellock, A. J.; Toney, M. F.; Hong, X.; Ahn, C. H.; and Chambers, S. A., "Ferromagnetism and structure of epitaxial Cr-doped anatase TiO2 thin films" (2006). *Xia Hong Publications*. 8.
https://digitalcommons.unl.edu/physicshong/8

This Article is brought to you for free and open access by the Research Papers in Physics and Astronomy at DigitalCommons@University of Nebraska - Lincoln. It has been accepted for inclusion in Xia Hong Publications by an authorized administrator of DigitalCommons@University of Nebraska - Lincoln.

Authors
T. C. Kaspar, T. Droubay, V. Shutthanandan, S. M. Heald, C. M. Wang, D. E. McCready, S. Thevuthasan, J. D. Bryan, D. R. Gamelin, A. J. Kellock, M. F. Toney, X. Hong, C. H. Ahn, and S. A. Chambers

This article is available at DigitalCommons@University of Nebraska - Lincoln: https://digitalcommons.unl.edu/physicshong/8

Ferromagnetism and structure of epitaxial Cr-doped anatase TiO_2 thin films

T. C. Kaspar,[1] T. Droubay,[1] V. Shutthanandan,[2] S. M. Heald,[1] C. M. Wang,[2] D. E. McCready,[2] S. Thevuthasan,[2] J. D. Bryan,[3] D. R. Gamelin,[3] A. J. Kellock,[4] M. F. Toney,[5] X. Hong,[6] C. H. Ahn,[6] and S. A. Chambers[1,*]

[1]*Fundamental Science Directorate, Pacific Northwest National Laboratory, Richland, Washington 99352, USA*

[2]*Environmental Molecular Sciences Laboratory, Pacific Northwest National Laboratory, Richland, Washington 99352, USA*

[3]*Department of Chemistry, University of Washington, Seattle, Washington 98195, USA*

[4]*IBM Almaden Research Center, San Jose, California 95120, USA*

[5]*Stanford Synchrotron Radiation Laboratory, Stanford Linear Accelerator Center, Menlo Park, California 94025, USA*

[6]*Department of Applied Physics, Yale University, New Haven, Connecticut 06520, USA*

(Received 22 December 2005; revised manuscript received 3 March 2006; published 24 April 2006)

The materials and magnetic properties of Cr-doped anatase TiO_2 thin films deposited on $LaAlO_3(001)$ and $SrTiO_3(001)$ substrates by oxygen-plasma-assisted molecular beam epitaxy have been studied in detail to elucidate the origin of ferromagnetic ordering. Cr substitution for Ti in the anatase lattice, with no evidence of Cr interstitials, segregation, or secondary phases, was independently confirmed by transmission electron microscopy with energy dispersive x-ray spectroscopy, extended x-ray absorption fine structure, and Rutherford backscattering spectrometry in the channeling geometry. Epitaxial films deposited at ~0.1 Å/s were found to have a highly defected crystalline structure, as quantified by high-resolution x-ray diffraction (XRD). These films were also ferromagnetic at room temperature with a moment of $\sim 0.5\mu_B$/Cr, Curie temperatures in the range of 400–700 °C, and exhibited shape and in-plane magnetocrystalline anisotropy. However, no free carrier spin polarization was observed by Hall effect measurements, raising questions about the mechanism of magnetism. Films deposited slowly (~0.015 Å/s) possessed a nearly perfect crystalline structure as characterized by XRD. Contrary to expectations, these films exhibited negligible ferromagnetism at all Cr concentrations. Annealing in vacuum to generate additional oxygen defects and free carrier electrons did not significantly increase the ferromagnetic ordering in either fast- or slow-grown films. These results contradict both oxygen-vacancy-derived free-carrier-mediated exchange and F-center-mediated bound magnetic polaron exchange mechanisms, and instead indicate the primary role of extended structural defects in mediating the ferromagnetic ordering in doped anatase films.

DOI: 10.1103/PhysRevB.73.155327 PACS number(s): 75.50.Pp, 75.25.+z, 85.75.−d

I. INTRODUCTION

Discovering and understanding materials for efficient spin injection into semiconductors in proposed spintronic devices presents a unique challenge. Suitable spin injectors must possess long-lived spin-polarized free carriers at and above room temperature, and these carriers must be able to cross the interface into the conventional semiconductor while maintaining a high degree of spin polarization. Ferromagnetic metals, such as Fe, exhibit reasonably high spin polarization well above room temperature, but their use in spintronic devices is limited by inefficient spin injection into semiconductors.[1] Attention has thus turned to dilute magnetic semiconductors (DMSs), for which the conductivity can be tuned to match that of the nonmagnetic semiconductor, resulting in maximum spin injection efficiency into the semiconductor heterostructure. While Mn-doped GaAs remains the prototypical ferromagnetic DMS, a low Curie temperature of no more than ~170 K to date prevents its use in practical room-temperature devices.[2] More promising for practical applications are transition-metal-doped semiconducting oxides, such as TiO_2, ZnO, and SnO_2, which have received considerable attention in the last several years due to many reports of room-temperature ferromagnetism in various dopant/oxide systems.[3–6] However, divergent ranges of reported properties for particular dopant/host combinations have hindered the fundamental understanding of these materials as well as their use in prototype spintronic devices.[5,6]

While hole-mediated ferromagnetic ordering appears to be operative in doped III-V compounds, such as Mn:GaAs,[2] the mechanism of ferromagnetism in doped transition-metal oxides is still under debate. Superexchange, double exchange, free-carrier-mediated exchange, and exchange through bound magnetic polarons (BMPs) have all been invoked to explain the ferromagnetic ordering above room temperature.[7–15] The often-cited BMP model has been discussed for III-V materials,[16,17] and extended by Coey *et al.*[3] to doped oxides. In oxides, the F-center-mediated BMP (FC BMP) model assumes that a bound electron (F center) arises from the oxygen vacancy created to maintain charge neutrality with the incorporation of an aliovalent dopant. The bound electron occupies a Bohr orbit whose radius is governed by the binding energy of the dopant energy levels and the electronic structure of the host oxide, and as a bound polaron it mediates ferromagnetic ordering of dopants within this orbital volume. At a sufficiently high BMP concentration, the polarons overlap, resulting in a spin-polarized impurity band in the band gap and ferromagnetic ordering throughout the material. This simple model neatly explains the observed ferromagnetic behavior of both highly resistive and *n*-type semiconducting oxides. However, neither the FC BMP model nor any of the others mentioned above have been conclusively shown to be operant in any of the dopant/oxide systems investigated to date. Likewise, none of these models

 ©2006 The American Physical Society

explain the broad range of magnetic moment values which have been observed in all the dopant/oxide systems. Moments considerably smaller than those predicted by spin counting are generally obtained,[18] although moments significantly larger than the expected value have also been claimed.[13,19]

Although electronic point defects, such as antisites, interstitials, and vacancies, have been discussed in detail for doped III-V semiconductors,[2,20] little attention has been paid in any potential DMS system to the role of extended structural defects, such as dislocations, twin boundaries, and subgrain boundaries between tilted lattice planes. This omission is due to the tacit assumption that structural defects will detrimentally impact ferromagnetic ordering, regardless of the exchange mechanism, as observed in other magnetic systems.[21,22] In magnetic superexchange and double exchange models, which require near-neighbor electron transfer, structural defects are assumed to interrupt these ionic "chains." Likewise, carrier interactions in free carrier and FC BMP models are expected to be hindered or eliminated by structural defects that form deep electronic traps. The spin-polarized free carriers necessary for spin injection can be easily depolarized by structural defects, which have been shown experimentally to act as spin-flip centers.[23] Contrary to this assumption, however, we have recently shown that structural defects play a primary role in the ferromagnetic ordering of Cr-doped TiO_2 anatase, which only exhibits strong room-temperature ferromagnetism in defective films with significant mosaic spread.[24] This result implies that none of the common mechanisms of ferromagnetic ordering directly apply to $Cr:TiO_2$.

In this paper, we present a full and detailed report of our work on this system.[14,15,24] Cr-doped TiO_2 anatase was chosen as a model dilute ferromagnetic oxide semiconductor for several reasons. Anatase exhibits a high electron mobility[25] compared to other oxides, and can easily be reduced to an *n*-type semiconductor through the generation of oxygen vacancies and/or Ti interstitials.[26] Further, anatase is reasonably well lattice matched to Si, making it a prime candidate for future integration with Si-based devices.[27] Chromium has been shown to be a ferromagnetic dopant in several classes of semiconductors, such as II-VI,[28] III-N,[29,30] and V_2VI_3 (tetradymite).[31] In contrast to Co-doped TiO_2,[32] Cr distributes randomly in the anatase lattice, without evidence of segregation or clustering. Since Cr metal is antiferromagnetic, the presence of metal clusters will not generate a spurious magnetic signal. These properties make $Cr:TiO_2$ an attractive model system in which the observed materials and magnetic properties can be unambiguously attributed to a single phase of anatase in which a fraction of Ti has been replaced by Cr. Thus, we can now explore the fundamental property relationships in this system, with the goal of elucidating the mechanism of ferromagnetism.

II. EXPERIMENT

Thin films of epitaxial $Cr:TiO_2$ were deposited by oxygen-plasma-assisted molecular beam epitaxy (OPAMBE), as described previously.[15,33] Both electron-beam evaporation guns and high-temperature effusion cells were used to evaporate pure metal Ti and Cr. Atomic oxygen was supplied from an electron cyclotron resonance oxygen plasma source with an integrated ion trap.

Substrates were 1 cm $\times$ 1 cm $\times$ 1 mm thick single-crystal $LaAlO_3(001)$ (LAO, with a lattice mismatch to anatase of $\Delta a/a=-0.26\%$) and $SrTiO_3(001)$ (STO, $\Delta a/a=-3.1\%$). A 1 cm diameter circle of the polished surface was exposed for thin-film deposition. Partway through this work, it was discovered that a majority of the substrates, regardless of vendor, were contaminated with ferromagnetic material. This contamination most likely originated from the wafer dicing saw blade, and thus occurs primarily on the edges of the substrate. No contamination was ever observed on the epi-polished substrate surface when investigated by various spectroscopic techniques. Thus, most of the "fast-grown" samples (as defined below) were deposited on LAO substrates whose level of contamination had not been confirmed, although spot checks by vibrating sample magnetometry (VSM) on a few of the substrates before deposition indicated negligible ferromagnetic contamination. When magnetic contamination was checked for and detected, primarily later in the investigation, the measured magnetization was typically a fraction of that observed for fast-grown $Cr:TiO_2$ films. Therefore, the likely effect of magnetic contamination is an increase in the scatter of the saturation moment data for fast-grown films. Once the pervasive nature of ferromagnetic substrate contamination was understood, the contamination was eliminated from each subsequent substrate by etching the back and sides overnight in concentrated HNO_3, followed by rinsing and sonication in deionized water. Care was taken to avoid direct contact of the epi-polished top substrate surface with HNO_3, as contact with the acid was found to damage the surface. Removal of ferromagnetic contamination was confirmed by room-temperature VSM measured for every etched substrate. The "slow-grown" samples defined below were deposited on substrates which had undergone the HNO_3 etch treatment and were shown to exhibit no detectable ferromagnetism prior to growth.

Before introduction into the vacuum chamber, all substrates were cleaned by sonication in acetone and isopropanol and/or exposure in an ultraviolet-ozone cleaner. After loading into the OPAMBE chamber, substrates were exposed to the oxygen plasma at 2×10^{-5} Torr background pressure for 30 min to remove any residual adventitious carbon. To improve the crystalline order of the LAO substrate surface, most were annealed in the plasma at $\sim$550 °C for an additional 15–30 min.

LAO was used for most depositions since it has a better lattice match to anatase. STO was utilized when spectroscopic signals from La overlapped those of Cr or Ti. Two sets of deposition conditions were utilized, as described in Table I. For "fast" depositions, the anatase deposition rate was $\sim$0.1 Å/s at a substrate temperature of $\sim$700 °C. For "slow" depositions, the rate was reduced to $\sim$0.015 Å/s at a substrate temperature of $\sim$550 °C, which has been shown to result in atomically smooth pure anatase films.[34] In both cases, a buffer layer of pure TiO_2 was first deposited to establish the anatase lattice before the Cr shutter was opened. Layer-by-layer growth of anatase was verified by the obser-

TABLE I. OPAMBE deposition conditions for fast-grown and slow-grown epitaxial Cr-doped anatase thin films.

Conditions	Anatase rate (Å/s)	Substrate temperature (°C)	Oxygen pressure (Torr)	Film thickness (Å)	Ti source	Cr source
Fast	0.1	700	2×10^{-5}	200–1200	*e*-gun *k*-cell	*e*-gun
Slow	0.015	550	2×10^{-5}	450–550	*k*-cell	*k*-cell

vation of reflection high-energy electron diffraction (RHEED) intensity oscillations. In most cases, the RHEED oscillation frequency increased after the Cr shutter was opened,[15] although the magnitude of the increase did not always quantitatively scale with the Cr doping level. Immediately after deposition, the oxygen flux was stopped to prevent Cr diffusion to the film surface, as observed previously for Co-doped anatase.[35]

The surface crystallinity before, during, and after deposition was monitored in real time by RHEED. X-ray photoelectron spectroscopy (XPS), available *in situ* in an appended vacuum chamber, was utilized to confirm full oxidation of Ti as well as to provide an estimate of the Cr doping level and charge state. Film thickness and composition were confirmed by Rutherford backscattering spectrometry (RBS). RBS in the channeling geometry provided information on crystalline quality and Cr site occupation. The detailed crystalline structure was analyzed by high-resolution x-ray diffraction (XRD) with a four-circle goniometer and a double-crystal Ge(220) four-bounce monochromator. Two modes were used for the diffracted beam analyzer: Either a double-crystal Ge(220) analyzer or a 0.25° slit. High-resolution transmission electron microscopy (HRTEM) and energy-dispersive x-ray (EDX) spectroscopy were utilized to determine the precise microcrystalline structure and distribution of Cr within the film, respectively.

K-edge x-ray absorption near-edge spectroscopy (XANES) and extended x-ray absorption fine structure (EXAFS) were measured on the PNC-CAT beamlines at the Advanced Photon Source at Argonne National Laboratory to determine dopant charge state and local structural environment. Measurements were made with the x-ray polarization along the film surface to probe the bonding in the *a*-*b* plane of anatase and with the polarization perpendicular to the surface to probe the bonding along the *c* axis. Anomalous Hall measurements were made to assess spin polarization, using a Quantum Design Physical Properties Measurement System (PPMS).

Magnetic properties were measured at room temperature with a Lakeshore 7404 VSM. Unless noted otherwise, measurements were made with the magnetic field parallel to the film plane. The Curie temperature was measured with the high-temperature oven attachment, which utilizes heated flowing argon for temperature control. A superconducting quantum interference device (SQUID) spectrometer was utilized for low-temperature magnetic measurements.

III. RESULTS AND DISCUSSION

A. Materials characterization

The deposition of Cr-doped TiO_2 was monitored *in situ* by RHEED. For the fast-grown films, RHEED intensity oscillations were observed for most but not all depositions. In most cases, the oscillations which occurred during deposition of the pure TiO_2 buffer layer damped out soon after the Cr shutter was opened, as shown in Fig. 1. Regardless of oscillation behavior, fast-grown films exhibited a spotty RHEED pattern at the end of the growth, indicating a rough surface. In contrast, slow-grown films consistently exhibited RHEED oscillations that persisted well after the Cr shutter was opened. In some cases, the oscillations continued until nearly the end of the deposition. However, the final RHEED patterns exhibited more variability than the fast-grown films. Shown in Fig. 1 is a final RHEED pattern for a slow-grown film; a faint 4×1 reconstruction can be seen in the anatase

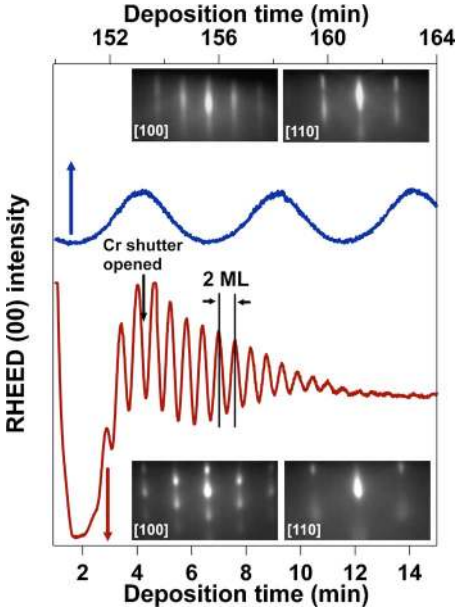

FIG. 1. (Color online) RHEED (00) intensity oscillations along the [100] azimuth of anatase and final RHEED patterns along the [100] and [110] azimuths for slow-grown 7% $Cr:TiO_2$ deposited on LAO at ~0.015 Å/s (top), and fast-grown 14% $Cr:TiO_2$ deposited on LAO at ~0.1 Å/s (bottom). For the fast-grown film (bottom), the arrow indicates when the Cr source shutter was opened to begin deposition of $Cr:TiO_2$; the Cr shutter was already open when the oscillations for the slow-grown material (top) were collected.

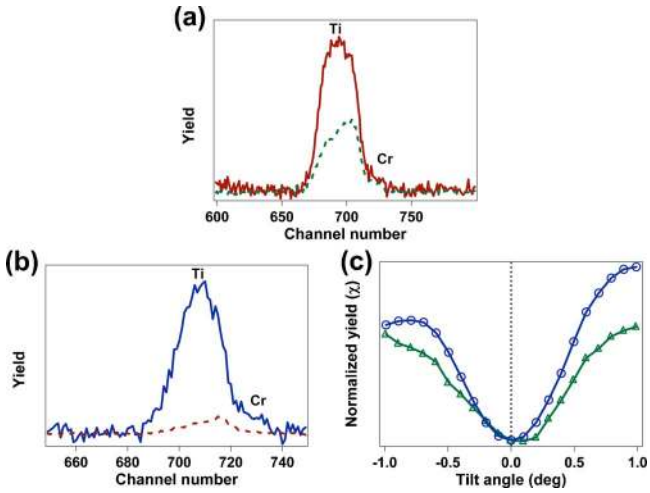

FIG. 2. (Color online) RBS random (solid lines) and channeling (dotted lines) measurements with the 2 MeV He^+ incident beam normal to the surface. (a) Channeling minimum yields for 825 Å of fast-grown 6% $Cr:TiO_2$/LAO were 38% for Ti and 59% for Cr. (b) Minimum yields for 465 Å of slow-grown 7% $Cr:TiO_2$/LAO were 8% for Ti and 9% for Cr. (c) Channeling rocking curve of slow-grown sample. Coincidence of minima for Ti (circles) and Cr (triangles) indicates Cr occupies the same cation position as Ti in the anatase lattice.

[100] azimuth, indicating an exceptionally flat, well-ordered anatase surface.[34] Other slow-grown films exhibited modulation along the streaks, indicative of a rougher surface. This variability in surface smoothness probably results from variations in substrate surface quality and/or substrate twinning.

The detailed crystalline structure and morphology observed by HRTEM and high-resolution XRD has been discussed in detail previously for both fast-grown[14,15] and slow-grown[24] $Cr:TiO_2$. Briefly, the fast-grown films were found to be epitaxial with nanoscale surface roughness, which corresponds to structural defects that extend through the film. This defect structure was also manifested by a large XRD rocking curve peak width, which indicates a significant mosaic structure in the film.[36] A substantial improvement in crystalline quality was observed for slow-grown material, with a nearly atomically flat surface, few extended defects, and a very narrow rocking curve peak width. Compositional analysis by EDX confirmed a uniform distribution of Cr for either deposition condition, with no evidence of significant Cr segregation, secondary phases, or Cr metal inclusions.

RBS in the channeling geometry has also been utilized to assess crystallinity. In addition, channeling provides information on Cr site occupancy. RBS channeling results in the ⟨001⟩ direction (normal to the film surface) are presented in Fig. 2. As expected, the degraded crystalline order in the fast-grown film is evidenced by relatively high channeling minimum yields. For several fast-grown films, the minimum yields were >40% for both Ti and Cr. The similarity in the minimum yields for both Ti and Cr indicates that Cr has substituted for Ti in the anatase lattice with equal proportions of each distorted from their ideal geometry. Much lower minimum yields were obtained for a slow-grown film (8% for Ti and 9% for Cr), indicating significantly less static disorder in the lattice. Again, the similar minimum yields are a strong indication that Cr substitutes for Ti in the lattice. Further evidence of Cr substitution is found in the coincidence of channeling minima for Ti and Cr in the RBS rocking curve presented in Fig. 2(c), which rules out a significant fraction of Cr occupying interstitial sites. Channeling measurements along other directions, such as 67° off normal (not shown), also indicated, for one $Cr:TiO_2$ sample, Cr substitution for Ti without evidence of Cr interstitials. Another similar sample showed some evidence of interstitial Cr visible at 67°; however, this sample had experienced a significant amount of ion-beam damage which may have resulted in localized interstitial Cr formation. The presence of even a small quantity of Cr interstitials was not supported by EXAFS measurements for either sample, as discussed below.

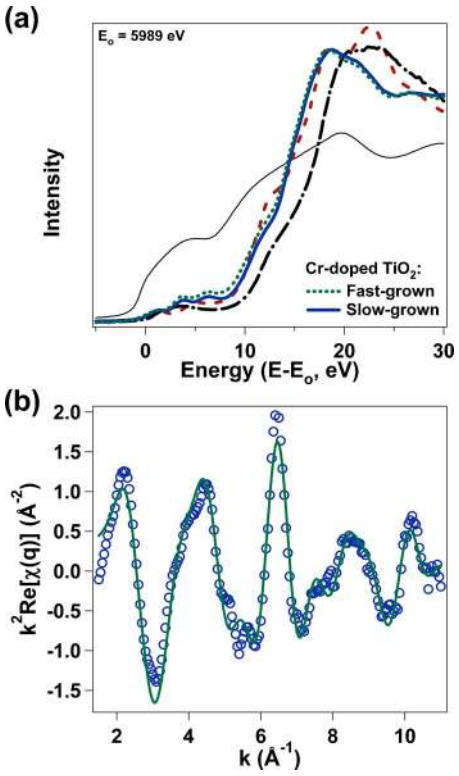

FIG. 3. (Color online) (a) Cr *K*-edge XANES spectra for fast-grown 9% $Cr:TiO_2$/LAO and slow-grown 8% $Cr:TiO_2$/STO, as well as standards of Cr metal (thin solid line), Cr_2O_3 (dashed), and CrO_2 (dashed-dotted). The inflection point energies of both $Cr:TiO_2$ spectra match that for Cr_2O_3, indicating Cr is present as Cr(III) in $Cr:TiO_2$. (b) k^2-weighted Cr *K*-edge EXAFS data for the slow-grown sample (circles) and fit to the data by FEFF calculations assuming Cr is substitutional in anatase (solid line).

The charge state of the Cr dopant can be probed sensitively with Cr *K*-edge XANES. In Fig. 3, the XANES spectra for both fast- and slow-grown samples are presented, along with the spectra for standards of Cr metal, α-Cr_2O_3, and CrO_2. It is evident that the spectra for the two $Cr:TiO_2$ films are very similar, indicating that Cr possesses the same charge state, in similar or identical surroundings, in both films. The absorption edges closely match that of Cr_2O_3, especially near the inflection point of the leading edge, indicating that Cr is

TABLE II. Parameters calculated by FEFF to best fit the experimental EXAFS data of several slow-grown $Cr:TiO_2$ films deposited on STO. R_{ab} and R_c are the Co–O nearest-neighbor bond lengths in the *a-b* and *c* planes of anatase, respectively, σ^2 are the Debye–Waller factors, and *N* are the number of nearest-neighbor anions. The FEFF model was based on substitutional Cr replacing Ti in the anatase lattice. For reference, the values for pure anatase TiO_2 and corundum Cr_2O_3 are also included.

Sample	R_{ab} (Å)	σ^2_{ab}	N_{ab}	R_c (Å)	σ^2_c	N_c	N_{total}
Ideal TiO_2	1.937		4	1.966		2	6
<2% Cr	1.95	0.0015	3.7	1.96	0.0022	1.9	5.6
3% Cr	1.96	0.0028	3.9	1.98	0.0029	1.7	5.6
8% Cr	1.97	0.0039	4.2	1.98	0.0022	1.6	5.8
Ideal α-Cr_2O_3	$R_1=1.96$ Å		3	$R_2=2.01$ Å		3	6

present predominantly as Cr(III) in both films. Aside from the chemical shift, the line shape of $Cr:TiO_2$ more closely resembles CrO_2 than Cr_2O_3, which is expected since anatase is more like the rutile structure of CrO_2 than the corundum structure of Cr_2O_3. Unfortunately, since the line shape of $Cr:TiO_2$ is significantly different from Cr_2O_3, a simple line shape analysis cannot be performed to quantify the potential contribution of a small fraction of Cr(IV) to the XANES spectrum,[37] and thus a small minority phase of Cr(IV) ($\lesssim$10% of the total Cr) cannot be ruled out. It is important to note that, if a minority of Cr(IV) is present, it is present at the same level in both fast- and slow-grown films. There is no experimental evidence to support an increased concentration of Cr(IV) in fast-grown $Cr:TiO_2$ relative to slow-grown material; thus, the presence of ferromagnetism in fast-grown $Cr:TiO_2$ cannot be attributed to Cr(IV) hybridization, as recently predicted by Ye *et al.*[38]

The specific environment around Cr can be explored with EXAFS. Figure 3(b) shows the k^2-weighted EXAFS spectrum for a slow-grown film deposited on STO, along with calculations utilizing the FEFF computer program[39] fit to the experimental data, assuming Cr substitutes for Ti in the anatase lattice. Simultaneous fitting of the two x-ray polarizations was carried out over the *k*-space range of 2–10.5 $Å^{-1}$ and the *r*-space range of 1–3.6 Å. The Co–O bond lengths (R_{ab} for the *a-b* plane of anatase and R_c for the *c* plane), Debye–Waller factors (σ^2), and coordination numbers (*N*) are given in Table II for three slow-grown $Cr:TiO_2$/STO samples. In all cases, the EXAFS data was well fit by the substitutional model. Other models were explored, such as adding a small fraction of Cr in an interstitial site, and the fits were significantly degraded. As indicated in Table II, the relatively short *k*-space range for fitting gave a significant correlation between the Debye–Waller factors and the coordination numbers. The fitted σ^2 values appear to be unusually low, which would result in reduced coordination numbers. For comparison, the Cr–O bond in Cr_2O_3 was found to have a Debye–Waller factor of $\sigma^2=0.0038$, somewhat larger than the values obtained for $Cr:TiO_2$. Therefore, it is likely that the fitted coordination numbers of 5.6–5.8 for $Cr:TiO_2$ may also be somewhat low. Even with this reduction, however, the coordination numbers are not sufficiently low to be indicative of charge-compensating oxygen vacancies adjacent to Cr. For instance, when $x=0.08$ in $Cr_xTi_{1-x}O_{2-x/2}$, *N* would be 5.0 if each vacancy were directly adjacent to a substitutional Cr, and would be 5.9 if the compensating oxygen vacancies were present but randomly distributed throughout the lattice. On average, a value of ~5.4 is expected if approximately one-half of the vacancies have Cr dopants as nearest neighbors. The fact that $N=5.8$ for $x=0.08$ indicates that the vacancies are randomly distributed throughout the lattice and therefore not detectable by EXAFS. An alternative interpretation of this result is that oxygen vacancies are not the primary charge compensation mechanism in $Cr:TiO_2$, and instead charge neutrality is maintained by another route, such as Ti interstitials. Six-coordinate Cr(III), without evidence of five-coordinate species associated with neighboring oxygen vacancies, has also been confirmed by optical absorption spectroscopy and ligand field analysis for $Cr:TiO_2$ nanocrystals.[40] Although interference with the La *L* edge prevented quantitative fitting by FEFF, the EXAFS spectrum[24] for a fast-grown film deposited on LAO is very similar to the spectrum for the slow-grown material, which implies that Cr substitutes for Ti in the fast-grown samples as well.

From the results presented above, several generalizations can be made about $Cr:TiO_2$ deposited by OPAMBE, regardless of deposition rate:

(1) Cr is distributed throughout the anatase lattice without evidence of segregation or secondary phases.

(2) Cr substitutes for Ti in the lattice, and does not appear to occupy interstitial sites.

(3) Cr is present as predominantly Cr(III).

The primary difference between films grown fast (~0.1 Å/s) and slow (~0.015 Å/s) is crystalline quality. Although both deposition rates result in phase-pure epitaxial anatase films, the fast-grown films have a significant mosaic structure, indicating a considerable density of extended structural defects, while the slow-grown films have a well-ordered crystalline structure with few structural defects.

B. Magnetic properties

Figure 4(a) presents a plot of saturation moment measured in-plane by VSM at room temperature for several fast-grown $Cr:TiO_2$ films. In general, fast-grown films are ferromagnetic at room temperature with an average moment of $\sim 0.5\mu_B$/Cr. The scatter in the measured magnetic moments

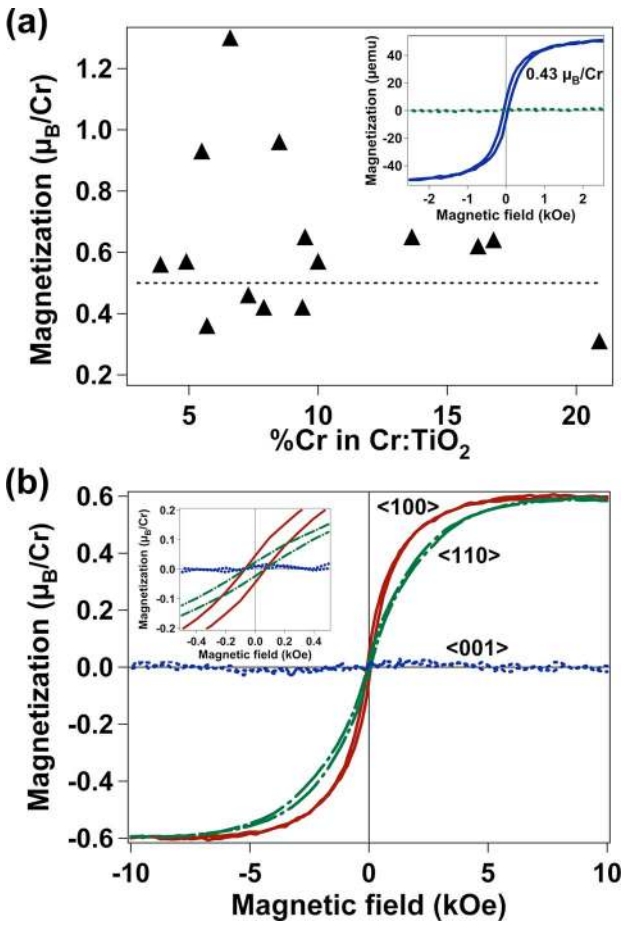

FIG. 4. (Color online) (a) Saturation moment per Cr dopant cation at room temperature for several fast-grown Cr:TiO_2 films of varying thicknesses and dopant concentrations. The dotted line represents the average saturation moment value of $0.5\mu_B$/Cr. Inset: Room-temperature hysteresis loops by VSM for a bare uncontaminated LAO substrate (dotted line) and after deposition of 560 Å of fast-grown 10% Cr:TiO_2 (solid line). (b) Hysteresis loops for fast-grown 9% Cr:TiO_2. The applied magnetic field was oriented along the crystallographic directions indicated (the ⟨100⟩ and ⟨110⟩ directions are in the plane of the film, while the ⟨001⟩ direction is perpendicular to the film plane). Both in-plane magnetocrystalline anisotropy and out-of-plane shape anisotropy are observed. Inset: Plot of the low-field region which shows hysteresis of the in-plane magnetization directions.

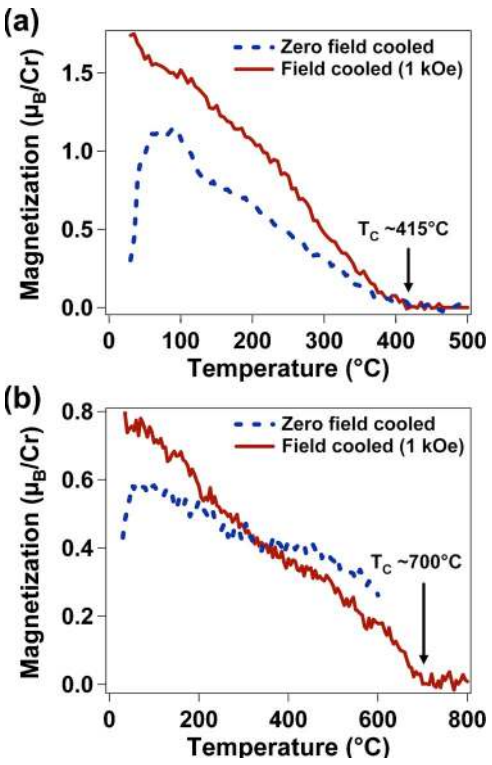

FIG. 5. (Color online) (a) Curie temperature measurement by VSM for one-half (1 cm × 0.5 cm) of fast-grown 8% Cr:TiO_2/LAO. ZFC data were obtained first; the sample was then cooled in a magnetic field of 1 kOe, and the measurement repeated. The Curie temperature was found to be ~415 °C for both measurements. (b) Curie temperature measurement by VSM for one-half of fast-grown 10% Cr:TiO_2/LAO. ZFC and FC data were collected as in (a). The Curie temperature was found to be ~700 °C.

may be due partly to small amounts of substrate contamination, as discussed in Sec. II. However, the prospect of substrate contamination cannot account for all (or even a majority of) the measured ferromagnetic signal, given the narrow range of saturation moments measured for most samples ($0.3–0.7\mu_B$/Cr), over a wide range of film thicknesses (200–1200 Å) and dopant concentrations (4–20% Cr). The three data points greater than $\sim 0.9\mu_B$/Cr are most likely outliers due to significant ferromagnetic substrate contamination and were discarded from further analysis. The inset to Fig. 4(a) shows the room-temperature VSM hysteresis loop for a bare LAO substrate that has been etched to remove ferromagnetic contamination, and the same substrate after deposition of 560 Å 10% Cr:TiO_2; the ferromagnetic hysteresis for the film provides clear confirmation that Cr:TiO_2 is ferromagnetic at room temperature in the absence of substrate contamination. Figure 4(b) plots the hysteresis loops for several orientations of a 9% Cr:TiO_2 film relative to the applied magnetic field of the VSM. In-plane magnetocrystalline anisotropy is observed, providing strong evidence that the ferromagnetic ordering is coupled to the anatase lattice. In the plane of the film, the ⟨100⟩ direction is an easy axis relative to the ⟨110⟩ direction. Additionally, essentially no out-of-plane ferromagnetism is observed, consistent with shape anisotropy from a thin film disk (425 Å thick) whose easy axes lie in plane.[41]

Measurements of the Curie temperature by VSM reveal the robust nature of the ferromagnetic ordering in fast-grown Cr:TiO_2, as presented in Fig. 5(a). In the zero-field-cooled (ZFC) mode, initial sample heating in an applied magnetic field of 5 kOe significantly increased the ferromagnetic signal, with a peak at ~80 °C. This behavior is reminiscent of a collection of superparamagnetic particles, in which the magnetization peak would correspond to the blocking temperature, T_B, above which thermal fluctuations dominate over magnetocrystalline anisotropy and thus the magnetization in the particles spontaneously switches direction. For this case, an estimation of the particle size can be made from the anisotropy energy and observed blocking temperature:[42,43]

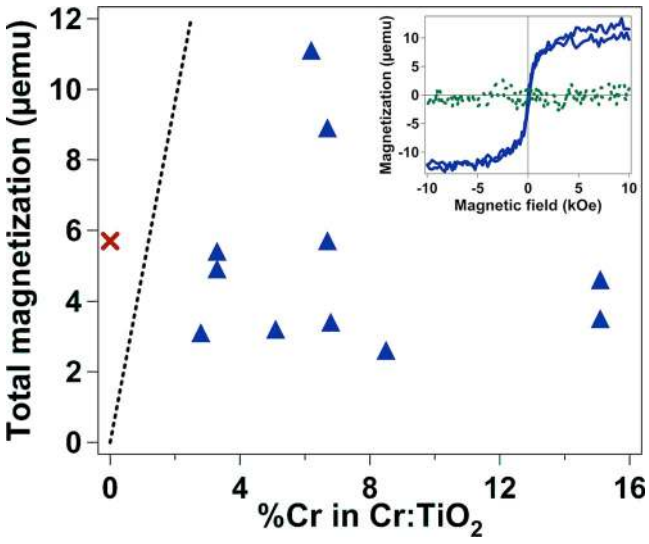

FIG. 6. (Color online) Total measured magnetization by VSM at room temperature for several slow-grown $Cr:TiO_2$ films of approximately 450 Å thickness and varying dopant concentrations. The total magnetization does not appear to correlate to Cr dopant concentration. The dotted line is the expected magnetization for a 450 Å thick $Cr:TiO_2$ film assuming a saturation moment of $0.5\mu_B$/Cr. The **x** symbol represents the total measured magnetization of a pure anatase thin film with no Cr dopant. Inset: VSM hysteresis loops for a bare LAO substrate (dotted line) and after deposition of 450 Å 6% $Cr:TiO_2$ (solid line).

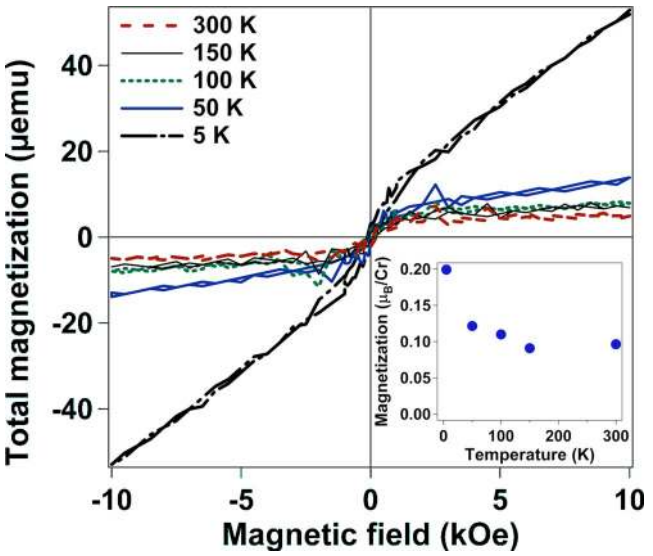

FIG. 7. (Color online) Hysteresis loops by SQUID magnetometry as a function of temperature for slow-grown 8% $Cr:TiO_2$/LAO. The diamagnetic background signal from the LAO substrate has been subtracted. A large paramagnetic contribution is evident at temperatures <50 K. Shown in the inset is the extracted ferromagnetic saturation moment, defined as the y intercept of the linear portion of the loops shown in the figure.

$$K_A V = 25 k_B T_B, \tag{1}$$

where K_A is the magnetocrystalline anisotropy energy density, V is the particle volume, and k_B is the Boltzmann constant. The only likely ferromagnetic (and thus potentially superparamagnetic) secondary phase in the Cr–Ti–O system is CrO_2. Assuming that the superparamagnetic particles are CrO_2 with an anisotropy density[44] of $K_A = 2.6 \times 10^5$ erg/cm^3 and an observed blocking temperature of $T_B = 355$ K, the estimated CrO_2 particle diameter from Eq. (1) would be $\sim$200 Å. CrO_2 particles this size would be easily observed; instead, we see no evidence of them by HRTEM or XRD, and no Cr(IV) is detected by XANES. We conclude that the peak in magnetization with temperature is not due to a collection of superparamagnetic CrO_2 particles, and instead likely results from overcoming in-plane shape anisotropy in $Cr:TiO_2$, since the magnetic field is applied along the short in-plane direction of the half-sample. As the temperature is further increased, the ferromagnetic signal drops until the Curie temperature of $\sim$415 °C is reached. It should be noted that this temperature is far from the expected value for potential secondary phases, such as CrO_2 ($T_C = 113$ °C). After cooling the sample in a magnetic field of 1 kOe (field-cooled or FC mode), the measurements were repeated. Due to the artificial anisotropy imposed by the external magnetic field during cooling, the sample exhibited a stronger magnetic signal at room temperature than the preceding ZFC measurement. As the temperature was increased, the magnetic signal decreased monotonically until the Curie temperature was reached. Again, this temperature was found to be $\sim$415 °C.

Figure 5(b) presents the ZFC and FC magnetization data for fast-grown 10% $Cr:TiO_2$, which exhibited qualitatively similar behavior to the film shown in Fig. 5(a). Upon initial heating (ZFC mode), shape anisotropy was overcome, resulting in a modest increase in the ferromagnetic moment. Further heating reduced the saturation moment. The Curie point had not been passed when the temperature reached 600 °C. However, the experiment was stopped to prevent any irreversible material change that may occur at high temperature. The sample was then cooled in a field of 1 kOe, and the measurement was repeated, this time going past the Curie point. In this case, the Curie temperature was found to be $\sim$700 °C.

While the magnetic properties of fast-grown $Cr:TiO_2$ are promising, the measured moment per Cr ($\sim 0.5\mu_B$/Cr) is still significantly less than the spin-only value of $3\mu_B$/Cr for Cr(III), which is a d^3 system. In an attempt to increase the magnetic moment per Cr, we investigated slow-grown $Cr:TiO_2$, with the assumption that the improved crystallinity would correspond to increased ferromagnetic ordering and thus a higher moment per Cr. However, as shown in Fig. 6, exactly the opposite proved to be true. Slow-grown $Cr:TiO_2$ exhibits significantly *reduced* ferromagnetic ordering compared to fast-grown material, with most saturation moment values in the range of $0.05–0.15\mu_B$/Cr. For a typical slow-grown film thickness of 450 Å, this corresponds to a total magnetic signal of less than 10 μemu. These measured values are near the sensitivity limit of the VSM, and thus cannot be attributed with any confidence to intrinsic ferromagnetism in the slow-grown $Cr:TiO_2$ films. As an illustration of this point, an *undoped* slow-grown anatase film is also plotted in Fig. 6. This specimen exhibited a total moment comparable to those of doped slow-grown films, suggesting that the mea-

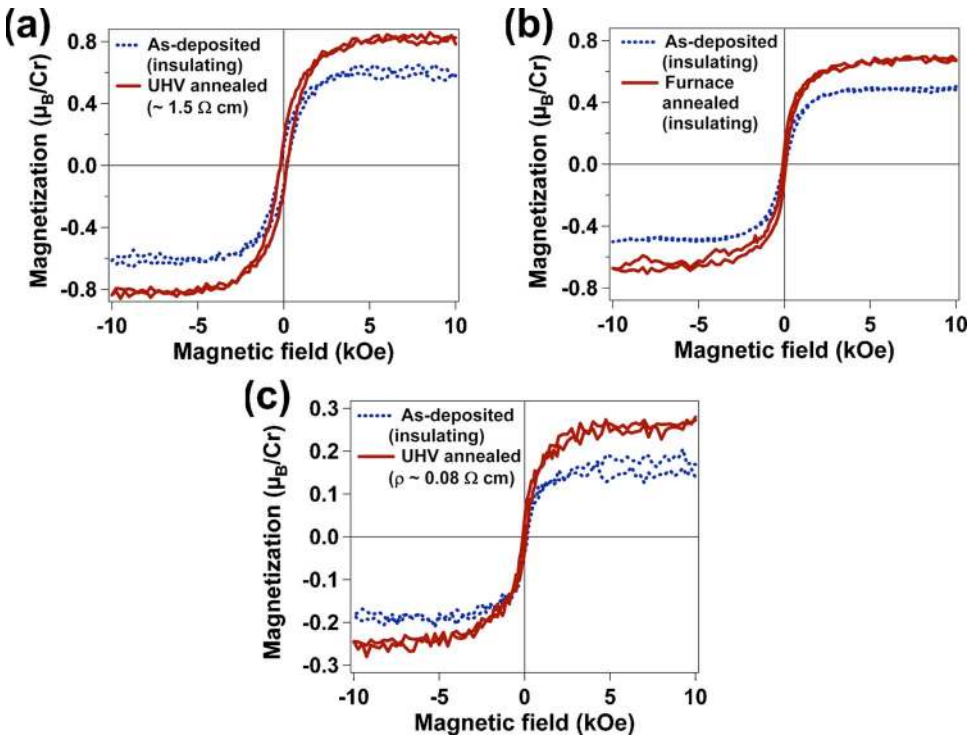

FIG. 8. (Color online) Room-temperature VSM hysteresis loops of $Cr:TiO_2$/LAO films as deposited (dotted lines) and after annealing (solid lines). Resistivity values determined by four-point probe conductivity. (a) Fast-grown 6% $Cr:TiO_2$ as deposited and after annealing in UHV at 600 °C for several hours, resulting in a resistivity of ~1.5 Ω cm. (b) Fast-grown 16% $Cr:TiO_2$ as-deposited and after annealing at 600–650 °C in a tube furnace with flowing N_2. Resistivity after annealing was still too high to measure with the four-point probe apparatus. (c) Slow-grown 6% $Cr:TiO_2$ as-deposited and after annealing in UHV at 550 °C for several hours, resulting in a resistivity of ~0.08 Ω cm.

sured signal may originate from magnetic contamination of an unknown origin, which may be introduced or activated during deposition. However, it is clear from Fig. 6 that, contrary to all expectations, slow-grown material does not exhibit the stronger magnetization observed in fast-grown films.

One potential explanation for the negligible room temperature ferromagnetism in slow-grown $Cr:TiO_2$ is that the Curie temperature is now below room temperature. Low-temperature SQUID measurements were utilized to investigate this possibility. As shown in Fig. 7, the ferromagnetic moment, defined as the intercept of the linear portion of the loop with the y axis, increases slightly from approximately $0.1\mu_B$/Cr to $0.2\mu_B$/Cr as the temperature is cooled to 5 K; again, however, these values are close to the sensitivity limit of the SQUID magnetometer and may not represent true ferromagnetism originating in the film. Hysteresis loops corresponding to a strongly ordered ferromagnetic phase of $0.5\mu_B$/Cr or greater are not obtained as the sample is cooled. In addition, a large paramagnetic contribution appears below 50 K, as indicated by an increased slope in the background signal. A significant number of paramagnetic spins may imply that the Cr ions are paramagnetic, as opposed to forming antiferromagnetic complexes. Unfortunately, the potential paramagnetic contribution from Cr ions in the films could not be determined due to the large number of paramagnetic rare-earth impurities in the LAO substrates.

Oxygen vacancy defects and their associated electrons, whether free[4] or bound in F-centers as BMPs,[3] have been suspected of playing an important role in the ferromagnetic ordering of dilute doped oxides. To explore the effect of oxygen defects and carriers in $Cr:TiO_2$, several films were annealed to introduce additional oxygen vacancy defects. All $Cr:TiO_2$ films are highly resistive ($\rho > \sim 5$ kΩ cm) as grown, as measured by four-point probe conductivity. After annealing at 550–600 °C for several hours in ultrahigh vacuum (UHV), both fast- and slow-grown films exhibit significantly reduced resistivity due to the loss of oxygen; each oxygen atom vacancy defect liberates two electrons that become free carriers. As illustrated in Figs. 8(a) and 8(c), after reduction to achieve resistivity values on the order of ~1.0–0.1 Ω cm, only a modest increase of 20–30% in the ferromagnetic signal is observed. Notably, the addition of free carriers to the slow-grown film did not increase its ferromagnetism to the level of the fast-grown film. Likewise, annealing a fast-grown sample at 600–650 °C in a tube furnace with flowing N_2 for several hours also results in a small increase in the ferromagnetic signal, as seen in Fig. 8(b). However, in this case, the film does not exhibit an increase in conductivity (within the measurement limit of the four-point probe apparatus). It is important to note that no change is observed in the XPS or Cr K-edge XANES spectra after heat treatment. These results imply that carrier-mediated exchange is not the primary mechanism of ferromagnetic ordering in $Cr:TiO_2$. Similarly, if the electrons associated with the oxygen vacancy become trapped to form FC BMPs, as may be the case in the tube furnace anneal, these FC BMPs do not appear to significantly increase the ferromagnetic ex-

change between Cr ions. Although the modest increase in the ferromagnetic signal after annealing may be related to ferromagnetic exchange mediated by free carriers or FC BMPs, these mechanisms appear to be only of secondary importance.

Overall, these magnetic results present a counterintuitive picture of ferromagnetism in $Cr:TiO_2$. Both the fast- and slow-grown $Cr:TiO_2$ films contain substitutional Cr(III) that is distributed throughout the lattice. The primary difference is that the fast-grown films have a significantly defected crystal structure, while the slow-grown films show few defects. Thus, the ferromagnetism observed in the fast-grown samples appears to be related to these structural defects. The question naturally arises as to whether material with an intermediate concentration of extended structural defects shows an intermediate level of ferromagnetic ordering, or if strong magnetic ordering occurs once a critical concentration of defects is achieved. To explore this question, several $Cr:TiO_2$ films were deposited at growth rates intermediate between fast-grown films (~0.1 Å/s) and slow-grown films (~0.015 Å/s). A direct correlation between growth rate and film structure, as judged by RHEED patterns collected after deposition, could not be made, most likely due to the strong influence of the LAO substrate surface quality on the structure of the $Cr:TiO_2$ films. Instead, XRD measurements of the anatase film were utilized to quantify the crystalline quality. Figures 9(a)–9(e) show ω-2θ specular scans through the anatase(004) reflection. These data were obtained with the Ge(220) analyzer for Figs. 9(a), 9(c), and 9(d), and the 0.25° slit for Figs. 9(b) and 9(e), as described in Sec. II. The oscillations on either side of the primary diffraction peak are finite size fringes resulting from the finite thickness of the doped anatase film. The presence and persistence of these finite-size oscillations is a measure of the crystalline order of atomic planes perpendicular to the growth direction, with more oscillations indicative of higher crystalline quality. To quantify the difference in crystalline order between films, the data were fit to a model of the anatase film, with a phenomenological term included that damps the finite-size oscillations. The film interface quality along the growth direction is characterized by a root-mean-square roughness (σ_{XRD}, in Å) that is similar to the roughness used in x-ray reflectivity,[45] with high-quality films having low σ_{XRD} values. For the higher-quality films with many oscillations, the fits describe the data well. However, for the lower-quality films exhibiting few if any oscillations, the model fit is not as good due to the presence of slightly misaligned anatase(004) crystallites (often referred to as mosaic spread) that contribute intensity in addition to the primary diffraction peak. While the mosaic spread degrades the accuracy of the resulting fit, the poorer crystalline order is still reflected as a larger value of σ_{XRD}. Figures 9(a)–9(e) also show the final RHEED patterns after deposition for each film. As expected, there is a correlation between the crystalline quality as measured by σ_{XRD} and the surface roughness as judged by increasing modulation of the streaks in the RHEED patterns.

Additionally, the film quality, as assessed by σ_{XRD}, correlates with increased ferromagnetic ordering at room temperature, as seen in Fig. 9(f). The poorest crystalline quality film, with a σ_{XRD} of 25 Å, exhibits a saturation moment of

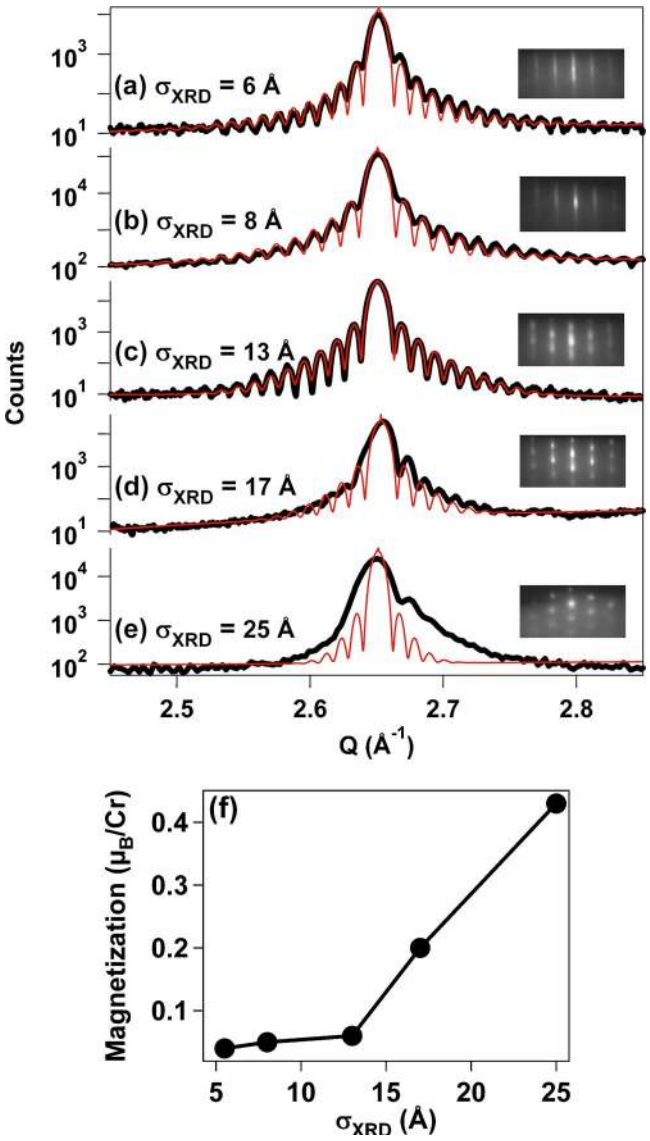

FIG. 9. (Color online) XRD ω-2θ scans for $Cr:TiO_2$/LAO films of varying crystalline quality, as well as final [100] azimuth RHEED patterns collected after deposition. (a) 508 Å, 12% Cr. (b) 465 Å, 7% Cr. (c) 453 Å, 8% Cr. The model fit overlaps the data almost exactly in this plot. (d) 497 Å, 7% Cr. (e) 567 Å, 10% Cr. (a), (c), and (d) were obtained with the Ge(220) analyzer; (b) and (e) were obtained with the 0.25° slit. (f) Plot of room-temperature saturation moment per Cr dopant versus the fitted roughness value σ_{XRD}. As the value of σ_{XRD} increases, the ferromagnetic saturation moment also increases.

$0.43\mu_B$/Cr, which is an order of magnitude greater than the highest crystalline quality film with a σ_{XRD} of 5.5 Å and saturation moment of $0.06\mu_B$/Cr. It appears from Fig. 9(f) that, once a critical structural defect level is reached, the increase in saturation moment is approximately linear with increasing σ_{XRD} values (decreasing crystalline quality). It would be optimal to include several more data points from $Cr:TiO_2$ films with different σ_{XRD} values to confirm the linear trend, but it is not feasible to reliably engineer the defect density of the films due to the observed lack of correlation between final crystalline quality and deposition rate. How-

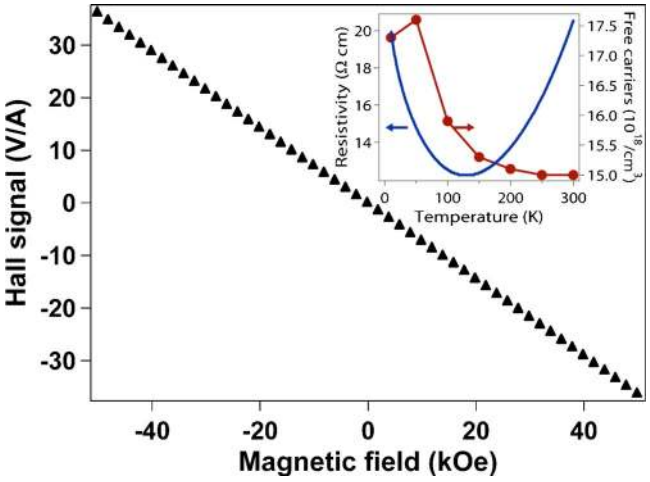

FIG. 10. (Color online) Anomalous Hall measurements at 10 K on a reduced fast-grown 8% $Cr:TiO_2$ sample show no anomalous Hall behavior. Inset: Resistivity (solid line) and free-carrier concentration (circles) from Hall measurements as a function of temperature.

ever, the linear relationship between crystalline quality and saturation moment would support a mechanism of ferromagnetic ordering arising directly from structural defects, such as the low-angle grain boundaries associated with mosaic spread, which are expected to increase proportional to the calculated σ_{XRD} value.

C. Spin polarization

The dopant spins are magnetically coupled to the free carrier band in a true ferromagnetic semiconductor, resulting in some measure of spin polarization. Thus, a determination of the free carrier spin polarization is of vital importance. Although it was shown above that free-carrier-mediated exchange is not the dominant mechanism of ferromagnetic ordering in $Cr:TiO_2$, this does not necessarily preclude the presence of spin-polarized free carriers in the material.[4] However, since all $Cr:TiO_2$ samples were highly resistive as grown, it was necessary to reduce the films in UHV for several hours at ~400–600 °C to produce measurable conductivity.

Free-carrier spin polarization can be observed as an anomalous component to Hall transport measurements at low values of the applied magnetic field. Since anomalous Hall behavior has also been observed for segregated metal particles in an oxide matrix,[42] it is considered a necessary but insufficient test for free carrier spin polarization in potential DMS materials. As shown in the inset of Fig. 10, fast-grown, vacuum-reduced 8% $Cr:TiO_2$ exhibits typical *n*-type semiconducting behavior,[25] with a resistivity minimum at ~130 K and $15–17.5\times10^{18}$ free carriers, although it is not clear why the apparent number of free carriers decreases with increasing temperature. As seen in Fig. 10, no anomalous Hall behavior is observed at 10 K. Cr-doped anatase does not appear to possess spin-polarized conduction-band free carriers, which may limit its usefulness as a spin injector.

D. Mechanism of ferromagnetism

The results presented above can assist in elucidating the mechanism of ferromagnetic ordering in $Cr:TiO_2$. Films deposited at a faster growth rate (~0.1 Å/s) were found to be consistently ferromagnetic at room temperature, with a saturation magnetization of $\sim0.5\mu_B$/Cr. The faster growth rate also resulted in poorer crystalline order in the films, as revealed qualitatively by TEM and quantitatively by XRD measurements. Slowing the deposition rate considerably (to ~0.015 Å/s) produced films with significantly better crystalline quality. However, the improved crystalline order did not correlate with improved ferromagnetic ordering; instead, slow-grown $Cr:TiO_2$ films exhibited negligible magnetism. This result is completely unexpected in light of the current theories of ferromagnetic ordering in doped oxides. It is tacitly assumed that extended structural defects will detrimentally affect ferromagnetic ordering, regardless of the details of the ferromagnetic exchange. Instead, this work shows that structural defects appear to play a primary role in promoting ferromagnetism in $Cr:TiO_2$. Ordering mediated by more conventional means, such as bulk-derived free-carrier electrons or FC BMPs, appear to be, at most, secondary mechanisms. These results demonstrate the imprudence of applying the model of free-carrier-mediated exchange to any semiconducting ferromagnetic oxide system, and likewise applying the FC BMP exchange model to any insulating ferromagnetic oxide system.

Recent total energy calculations support our experimental results.[38] This theoretical investigation revealed that substitutional Cr(III) dopants in anatase do not have a tendency to cluster, but are weakly interacting and form a paramagnetic ground state. These authors also predict that Cr(IV) dopants will strongly interact, at least at close distances, leading to a ferromagnetic ground state. They interpret the ferromagnetism in our fast-grown Cr-doped TiO_2 anatase as being due to undetectable Cr(IV). However, this explanation is difficult to reconcile with the fact that the Cr *K*-shell XANES spectra are essentially identical for fast- and slow-grown films, as discussed in Sec. III A. Given the sizeable difference in x-ray absorption threshold energy between Cr(III) and Cr(IV), we expect a measurable difference between spectra for films containing 100% Cr(III) and those containing $\leqslant\sim10\%$ Cr(IV)/$\geqslant\sim90\%$ Cr(III). Moreover, if the ferromagnetism is due to Cr(IV), and if only ~10% of the Cr is in the +4 oxidation state, the moment per *ferromagnetic* Cr(IV) would be $\sim5\mu_B$/Cr in a film for which the moment per Cr averaged over all Cr dopants is $\sim0.5\mu_B$/Cr. Such a result is unphysical in that the maximum spin-only moment per Cr(IV) is $2\mu_B$/Cr, and the orbital contribution is not expected to constitute the difference.

If our correlation between ferromagnetic ordering and extended structural defects is shown to apply generally to doped oxides, it would explain the inconsistency of magnetic properties reported in the literature. Recent results by our group have revealed essentially the same loss of ferromagnetism in slow-grown $Co:TiO_2$,[46] which illustrates the generality of the phenomena. Unfortunately, while the present work demonstrates the clear correlation between structural

imperfections and ferromagnetic ordering, it does not provide details either on the specific structural defects involved, or how these defects interact with the Cr dopants to promote ferromagnetic ordering. However, recent work by Bryan *et al.*[40] on Co- and Cr-doped anatase TiO_2 nanocrystals may provide some clues. In this study, it was found that aggregation of the doped anatase nanoparticles was necessary to induce ferromagnetic ordering. After ruling out domain size effects and material changes during thermal annealing, Bryan *et al.*[11,47] hypothesized that the ferromagnetic ordering was mediated by charged grain-boundary defects that were formed between individual nanoparticles during aggregation. Similar results were also obtained for Ni-doped ZnO and SnO_2 nanocrystals. The role of charged grain-boundary defects is also a plausible explanation for the ferromagnetic ordering in defective fast-grown $Cr:TiO_2$ thin films. While the nature of the responsible charged structural defects is still not clear, it is obvious from the data presented here that they are fundamentally different from bulk-derived oxygen vacancy defects, whether present to preserve charge neutrality or generated during vacuum annealing, both of which were shown to have little impact on the ferromagnetism. A deeper understanding of the origin of ferromagnetic ordering will require a concerted experimental and theoretical effort whose detail far exceeds the current work in doped oxide systems.

IV. CONCLUSIONS

The materials and magnetic properties of epitaxial Cr-doped anatase thin films deposited on $LaAlO_3$ and $SrTiO_3$ by OPAMBE were studied in detail. Cr(III) was found to substitute for Ti(IV) in the anatase lattice with uniform distribution. The crystalline quality depended on the deposition rate: Fast-grown films exhibited a defected microstructure with a significant mosaic spread, while slow-grown films had a nearly perfect crystalline structure. Fast-grown films were also strongly ferromagnetic at room temperature ($\sim 0.5\mu_B$/Cr), with Curie temperatures in the range of 400–700 °C. No spin polarization was observed in the conduction band of fast-grown $Cr:TiO_2$, which likely makes it unsuitable as a spin injector. Contrary to expectations, slow-grown films of Cr-doped TiO_2 with excellent crystallinity exhibited significantly less ferromagnetic ordering. The addition of carriers and/or FC BMPs during postgrowth annealing did not significantly increase the room-temperature ferromagnetism, which implies that these mechanisms of ferromagnetic ordering are of secondary importance. Extended structural defects appear to be necessary to promote ferromagnetic ordering in $Cr:TiO_2$. Similar results were recently obtained for thin film Co-doped anatase,[46] as well as doped TiO_2, ZnO, and SnO_2 nanocrystals,[11,40,47] suggesting the broad applicability of this mechanism.

ACKNOWLEDGMENTS

This work was performed in the Environmental Molecular Sciences Laboratory, a national scientific user facility sponsored by the Department of Energy's Office of Biological and Environmental Research and located at Pacific Northwest National Laboratory. This work was supported by the U.S. Department of Energy, Office of Science, Office of Basic Energy Sciences, Division of Materials Science and Engineering Physics under Project No. 10122. Work at UW was funded by the NSF (DMR-0239325 and ECS-0224138) and the Research Corporation. T.C.K. acknowledges support from the PNNL/University of Washington Joint Institute for Nanoscience. Hall effect measurements were carried out at Yale University. XRD measurements utilizing the diffracted beam monochromator were carried out at Stanford University. Use of the Advanced Photon Source was supported by the U.S. Department of Energy, Office of Science, Office of Basic Energy Sciences under Contract No. W-31-109-ENG-38.

*Electronic address: sa.chambers@pnl.gov

[1] G. Schmidt, D. Ferrand, L. W. Molencamp, A. T. Filip, and B. J. vanWees, Phys. Rev. B **62**, R4790 (2000).
[2] A. H. McDonald, P. Schiffer, and N. Samarth, Nat. Mater. **4**, 195 (2005).
[3] J. M. D. Coey, M. Venkatesan, and C. B. Fitzgerald, Nat. Mater. **4**, 173 (2005).
[4] S. J. Pearton, W. H. Heo, M. Ivill, D. P. Norton, and T. Steiner, Semicond. Sci. Technol. **19**, R59 (2004).
[5] R. Janisch, P. Gopal, and N. Spaldin, J. Phys.: Condens. Matter **17**, R657 (2005).
[6] T. Fukumura, H. Toyosaki, and Y. Yamada, Solid State Ionics **20**, S103 (2005).
[7] M. H. F. Sluiter, Y. Kawazoe, P. Sharma, A. Inoue, A. R. Raju, C. Rout, and U. V. Waghmare, Phys. Rev. Lett. **94**, 187204 (2005).
[8] M. S. Park, S. K. Kwon, and B. I. Min, Phys. Rev. B **65**, 161201(R) (2002).
[9] K. Sato and H. Katayama-Yoshida, Phys. Status Solidi B **229**, 673 (2002).
[10] D. A. Schwartz and D. R. Gamelin, Adv. Mater. (Weinheim, Ger.) **16**, 2115 (2004).
[11] P. V. Radovanovic and D. R. Gamelin, Phys. Rev. Lett. **91**, 157202 (2003).
[12] A. C. Tuan, J. D. Bryan, A. B. Pakhomov, V. Shutthanandan, S. Thevuthasan, D. E. McCready, D. Gaspar, M. H. Engelhard, J. W. Rogers, Jr., K. Krishnan, D. R. Gamelin, and S. A. Chambers, Phys. Rev. B **70**, 054424 (2004).
[13] J. M. D. Coey, A. P. Douvalis, C. B. Fitzgerald, and M. Venkatesan, Appl. Phys. Lett. **84**, 1332 (2004).
[14] T. Droubay, S. M. Heald, V. Shutthanandan, S. Thevuthasan, S. A. Chambers, and J. Osterwalder, J. Appl. Phys. **97**, 046103 (2005).
[15] J. Osterwalder, T. Droubay, T. Kaspar, J. Williams, C. M. Wang, and S. A. Chambers, Thin Solid Films **484**, 289 (2005).
[16] A. Kaminski and S. Das Sarma, Phys. Rev. Lett. **88**, 247202 (2002).

[17] A. C. Durst, R. N. Bhatt, and P. A. Wolff, Phys. Rev. B **65**, 235205 (2002).
[18] W. Prellier, A. Fouchet, and B. Mercey, J. Phys.: Condens. Matter **15**, R1583 (2003).
[19] S. B. Ogale, R. J. Choudhary, J. P. Buban, S. E. Lofland, S. R. Shinde, S. N. Kale, V. N. Kulkarni, J. Higgins, C. Lanci, J. R. Simpson, N. D. Browning, S. Das Sarma, H. D. Drew, R. L. Greene, and T. Venkatesan, Phys. Rev. Lett. **91**, 077205 (2003).
[20] C. Timm, J. Phys.: Condens. Matter **15**, R1865 (2003).
[21] A.-M. Haghiri-Gosnet and J.-P. Renard, J. Phys. D **36**, R127 (2003).
[22] R. F. C. Farrow, IBM J. Res. Dev. **42**, 43 (1998).
[23] R. M. Stroud, A. T. Hanbicki, Y. D. Park, G. Kioseoglou, A. G. Petukhov, B. T. Jonker, G. Itskos, and A. Petrou, Phys. Rev. Lett. **89**, 166602 (2002).
[24] T. C. Kaspar, S. M. Heald, C. M. Wang, J. D. Bryan, T. Droubay, V. Shutthanandan, S. Thevuthasan, D. E. McCready, A. J. Kellock, D. R. Gamelin, and S. A. Chambers, Phys. Rev. Lett. **95**, 217203 (2005).
[25] L. Forro, O. Chauvet, D. Emin, L. Zuppiroli, H. Berger, and F. Levy, J. Appl. Phys. **75**, 633 (1994).
[26] U. Diebold, Surf. Sci. Rep. **48**, 53 (2003).
[27] T. C. Kaspar, T. Droubay, C. M. Wang, S. M. Heald, A. S. Lea, and S. A. Chambers, J. Appl. Phys. **97**, 073511 (2005).
[28] H. Saito, V. Zayets, S. Yamagata, and K. Ando, Phys. Rev. B **66**, 081201(R) (2002).
[29] H. X. Liu, S. Y. Wu, R. K. Singh, L. Gu, D. J. Smith, N. Newman, N. R. Dilley, L. Montes, and M. B. Simmonds, Appl. Phys. Lett. **85**, 4076 (2004).
[30] R. M. Frazier, G. T. Thaler, J. Y. Leifer, J. K. Hite, B. P. Gila, C. R. Abernathy, and S. J. Pearton, Appl. Phys. Lett. **86**, 052101 (2005).
[31] J. S. Dyck, C. Drasar, P. Lost'ak, and C. Uher, Phys. Rev. B **71**, 115214 (2005).
[32] S. A. Chambers, T. Droubay, C. M. Wang, A. S. Lea, R. F. C. Farrow, L. Folks, V. Deline, and S. Anders, Appl. Phys. Lett. **82**, 1257 (2003).
[33] S. A. Chambers, Surf. Sci. Rep. **39**, 105 (2000).
[34] Y. Liang, S. Gan, S. A. Chambers, and E. I. Altman, Phys. Rev. B **63**, 235402 (2001).
[35] S. A. Chambers, S. Thevuthasan, R. F. C. Farrow, R. F. Marks, J. U. Thiele, L. Folks, M. G. Samant, A. J. Kellock, N. Ruzycki, D. L. Ederer, and U. Diebold, Appl. Phys. Lett. **79**, 3467 (2001).
[36] V. Srikant, J. S. Speck, and D. R. Clarke, J. Appl. Phys. **82**, 4286 (1997).
[37] V. Shutthanandan, S. Thevuthasan, S. M. Heald, T. Droubay, M. H. Engelhard, T. C. Kaspar, D. E. McCready, L. Saraf, S. A. Chambers, B. S. Mun, N. Hamdan, P. Nachimuthu, B. Taylor, R. P. Sears, and B. Sinkovic, Appl. Phys. Lett. **84**, 4466 (2004).
[38] L. H. Ye and A. J. Freeman, Phys. Rev. B **73**, 081304(R) (2006).
[39] S. I. Zabinsky, J. J. Rehr, A. Ankudinov, R. C. Albers, and M. J. Eller, Phys. Rev. B **52**, 2995 (1995).
[40] J. D. Bryan, S. A. Santangelo, S. C. Keveren, and D. R. Gamelin, J. Am. Chem. Soc. **127**, 15568 (2005).
[41] M. Volmer and J. Neamtu, J. Optoelectron. Adv. Mater. **5**, 319 (2003).
[42] S. R. Shinde, S. B. Ogale, J. S. Higgins, H. Zheng, A. J. Millis, V. N. Kulkarni, R. Ramesh, R. L. Greene, and T. Venkatesan, Phys. Rev. Lett. **92**, 166601 (2004).
[43] B. D. Cullity, *Introduction to Magnetic Materials* (Addison-Wesley, Menlo Park, CA, 1972).
[44] U. Netzelmann, J. Appl. Phys. **68**, 1800 (1990).
[45] M. Tolan, *X-ray Scattering from Soft-Matter Thin Films* (Springer, New York, 1999).
[46] T. C. Kaspar, T. Droubay, D. E. McCready, M. F. Toney, S. M. Heald, C. M. Wang, A. S. Lea, V. Shutthanandan, and S. A. Chambers (unpublished).
[47] P. I. Archer, P. V. Radovanovic, S. M. Heald, and D. R. Gamelin, J. Am. Chem. Soc. **127**, 14479 (2005).